

The Ionospheric Bubble Index deduced from magnetic field and plasma observations onboard *Swarm*

Jaehung Park¹, Max Noja¹, Claudia Stolle^{2*}, and Hermann Lühr¹

¹Helmholtz-Centre Potsdam, GFZ German Research Center for Geosciences, Section 2.3, Telegrafenberg, D-14473 Potsdam, Germany

²DTU Space, Technical University of Denmark, Elektrovej, 2800 Kgs. Lyngby, Denmark

(Received March 14, 2013; Revised August 15, 2013; Accepted August 21, 2013; Online published November 22, 2013)

In the post-sunset tropical ionospheric F-region plasma density often exhibits depletions, which are usually called equatorial plasma bubbles (EPBs). In this paper we give an overview of the *Swarm* Level 2 Ionospheric Bubble Index (IBI), which is a standard scientific data of the *Swarm* mission. This product called L2-IBI is generated from magnetic field and plasma observations onboard *Swarm*, and gives information as to whether a *Swarm* magnetic field observation is affected by EPBs. We validate the performance of the L2-IBI product by using magnetic field and plasma measurements from the CHAMP satellite, which provided observations similar to those of the *Swarm*. The L2-IBI product is of interest not only for ionospheric studies, but also for geomagnetic field modeling; modelers can de-select magnetic data which are affected by EPBs or other unphysical artifacts.

Key words: Plasma irregularity, equatorial ionosphere, topside ionosphere.

1. Introduction

At night-time (in particular, between sunset and midnight) the low-latitude (<30° magnetic latitude) ionospheric F-region (>200 km) often exhibits local plasma density depletions. Since their first discovery using ionosondes (Booker and Wells, 1938), the irregularities have been observed by a variety of techniques. All the different names currently used for the depletions are historically related with the different measurement techniques. Decameter-scale irregularities appear as diffuse echoes in the ionograms (e.g. Abdu *et al.*, 1983), which is related to the name, Equatorial Spread-F (ESF). Meter-scale irregularities generate ‘backscatter plumes’ (e.g. Miller *et al.*, 2010) in the Very-High-Frequency (VHF) radar maps. Hectometer or sub-kilometer-scale irregularities generate ‘scintillation’ of radio wave signals (e.g. Paul *et al.*, 2011). In airglow images the irregularities are identified as band-shaped intensity depletions (e.g. Martinis *et al.*, 2003; Kil *et al.*, 2004). Abrupt drops appear in satellite measurements of plasma density (e.g. Aggson *et al.*, 1996; Huang *et al.*, 2001; Burke *et al.*, 2004; Yokoyama *et al.*, 2011; Xiong *et al.*, 2012), which are related to the name, Equatorial Plasma Bubble (EPB).

These density irregularities can be harmful to radio communication between ground and satellites (e.g. Basu *et al.*, 2002; Nishioka *et al.*, 2011), for which the ionosphere acts

as a propagation medium. With the advent of the space communication era the climatology of plasma density depletions (hereafter, we use ‘EPB’ (Equatorial Plasma Bubble) as a generic name for the plasma density depletions) has gained more and more practical relevance.

As described above, traditional EPB diagnostic methods count on in-situ plasma density probes, optical imagers, or radio wave sounding. However, EPBs can also be detected from their diamagnetic effects. Regions of locally depleted plasma are characterized by enhanced magnetic field strength. It has only recently become possible to recover reliably the weak magnetic signals of EPBs. Using Flux-Gate Magnetometer (FGM) measurements on-board the Challenging Mini-Satellite Payload (CHAMP) Stolle *et al.* (2006) could reconstruct the well-known EPB climatology obtained earlier by traditional EPB diagnostic methods.

The basic physics and underlying assumptions for interpreting the diamagnetic effect have been described by, for example, Lühr *et al.* (2003). For local plasma irregularities such as EPBs we can assume a linear field line geometry. Then, the magnetic tension can be neglected in the momentum balance. Lühr *et al.* (2003) assumed that a change in plasma pressure has to be compensated to first order by an adjusted magnetic pressure, which means a total pressure balance across the irregularity walls.

$$\Delta \left(\frac{B^2}{2\mu_0} \right) + k_B \Delta [n_e (T_e + T_i)] = 0, \quad (1)$$

where B is the magnetic field strength, μ_0 is the permeability of free space, k_B is the Boltzmann constant, n_e is the electron density, T_e and T_i are electron and ion temperatures, respectively. The Δ sign denotes the spatial gradient of the respective ionospheric parameters. Since the ambient field strength is larger by four orders of magnitudes than

*Now at GFZ, German Research Center for Geoscience, Section 2.3, Telegrafenberg, D-14473 Potsdam, Germany.

the field change induced by EPBs, we can linearize Eq. (1) as follows:

$$\frac{B \cdot \Delta B}{\mu_0} \approx -k_B \Delta [n_e(T_e + T_i)], \quad (2)$$

If we solve Eq. (2) for the field change, the result is:

$$\Delta B \approx -\frac{\mu_0 k_B}{B} \Delta [n_e(T_e + T_i)] \approx -\frac{\mu_0 k_B}{B} (\Delta n_e) (T_e + T_i). \quad (3)$$

In the last part of Eq. (3) we assumed that the diamagnetic effect is approximately proportional to the change in electron density. This is reasonable since the plasma temperature change across EPB walls is expected to be significantly smaller than the density change. Using Hinotori satellite observations at altitudes around 600 km for high solar activity, Oyama *et al.* (1988, figure 10) showed that the electron temperature change across an EPB wall was mostly within $\pm 20\%$. On the other hand, typical density changes across EPBs reached almost an order of magnitude, which made the product of electron temperature and density generally lower inside than outside the EPB (Oyama *et al.*, 1988, figure 4). Park *et al.* (2008) also have quantitatively investigated the balance between magnetic and plasma pressures: according to their figure 6 the plasma density change across EPB walls (under the assumption of constant T_e and T_i) can explain a dominant part (60–80%) of the magnetic pressure change. Hence, the ΔB and Δn_e across EPB walls should exhibit high correlation, by which plasma density irregularities can be detected reliably in magnetic field data.

At 400 km altitude plasma irregularities and the corresponding diamagnetic deflections occur preferentially along two bands at about 10° in latitude away from the magnetic equator (e.g. Stolle *et al.*, 2006, figure 7). Since EPBs are commonly associated with magnetic field enhancements, this additional signal will contaminate global models of the geomagnetic field; in particular those for high-degree lithospheric fields. For that reason it may be useful to identify EPBs from in-situ magnetic observations and de-select EPBs in geomagnetic field modeling efforts, as has been done by Maus *et al.* (2007).

Inspired by the successful EPB identification approach using the CHAMP/FGM (Stolle *et al.*, 2006), the European Space Agency (ESA) decided to introduce the Ionospheric Bubble Index (IBI) as a standard Level 2 (L2) data product for the upcoming *Swarm* mission. In this paper we give a description of the L2-IBI product and the related processing algorithm. Subsequently the results are verified scientifically using CHAMP data. In Section 2 we briefly describe the relevant *Swarm* data and our EPB detection method. In Section 3 details of the L2-IBI product are outlined in terms of format and meaning of each parameter. Section 4 presents a scientific validation of the L2-IBI product using CHAMP data. Finally, results are summarized, and conclusions are drawn in Section 5.

2. Data Sets and Processing Approach

ESA's *Swarm* constellation is a geomagnetic field mission consisting of three satellites which carry an instrument suite similar to that of the CHAMP satellite (http://www.esa.int/Our_Activities/

[Observing_the_Earth / The_Living_Planet_Programme/Earth_Explorers/Swarm](http://www.esa.int/Our_Activities/Programme/Earth_Explorers/Swarm)). Two of the satellites will fly at an initial altitude of 450 km while the other one will be at a height of 530 km with slightly different inclination. A Vector Field Magnetometer (VFM) is sampling the three components of the geomagnetic field at a rate of 50 Hz, and the Absolute Scalar Magnetometer (ASM) provides high-resolution readings of the total field once per second. These two data sets are combined to give the very accurate vector magnetic field data product at a rate of 1 Hz. The combined data are provided as *Swarm* Level 1b, which means calibrated time series of *Swarm* observations. The Electric Field Instrument (EFI) measures plasma density, electron/ion temperatures, and ion drift. From the EFI Level 1b data products we use the plasma density for the EPB detection.

The automatic procedure for EPB detection largely follows the approach introduced by Stolle *et al.* (2006). First, the 2 Hz plasma density data are synchronized to the time tags of the 1 Hz magnetic field data by linear interpolation. Then, the geomagnetic field contributions from the Earth's core, crust, and magnetosphere are removed from the magnetic measurements. The three sources of geomagnetic fields are represented by models: e.g., the International Geomagnetic Reference Field (IGRF) for the core, Magnetic Field Model 7 (MF7: <http://www.geomag.us/models/MF7.html>) for the crust, and Pomme6 (<http://www.geomag.us/models/pomme6.html>) for the magnetospheric fields, respectively. During the *Swarm* mission more accurate models will replace the current ones. By subtracting the sum of these three contributions (hereafter the 'mean field') from the observed magnetic field vectors, we can isolate magnetic field variations originating from the ionosphere (hereafter the 'residual field'). The residual field is then converted into the Mean-Field-Aligned (MFA) coordinate system. We project the residual field onto the mean field vector to separate field-aligned variations (MFA Z-component, hereafter the 'residual strength') from those perpendicular to the mean field (MFA X- and Y-components). An example of the residual strength is shown in Fig. 1(a).

The L2-IBI processor then selects night-time (18–06 local time), low-latitude (geographic latitude (GLAT) $< 45^\circ$) passes, because EPBs are generally known to occur in that range (e.g. Stolle *et al.*, 2006, figures 7–8). A high-pass filter (-3 dB cutoff at the period of approximately 24 seconds) is applied to the residual strength, limiting the signal to a passband of approximately 0.04–0.5 Hz (0.5 Hz is the Nyquist frequency). The passband corresponds to wavelengths of 15–188 km, assuming the vehicle orbit speeds of about 7.5 km/s. This step further removes large-scale magnetic field variations that are not related to EPBs. For example, the electron density enhancement associated with the Equatorial Ionization Anomaly (EIA) also exhibits a diamagnetic effect (Lühr *et al.*, 2003), which has much larger scale lengths than typical EPBs. The filtered residual strength is shown in Fig. 1(b).

For further processing the filtered residual strength is rectified. The filtered/rectified residual strength (Fig. 1(c)) is then compared with an event detection threshold (e.g., 0.2

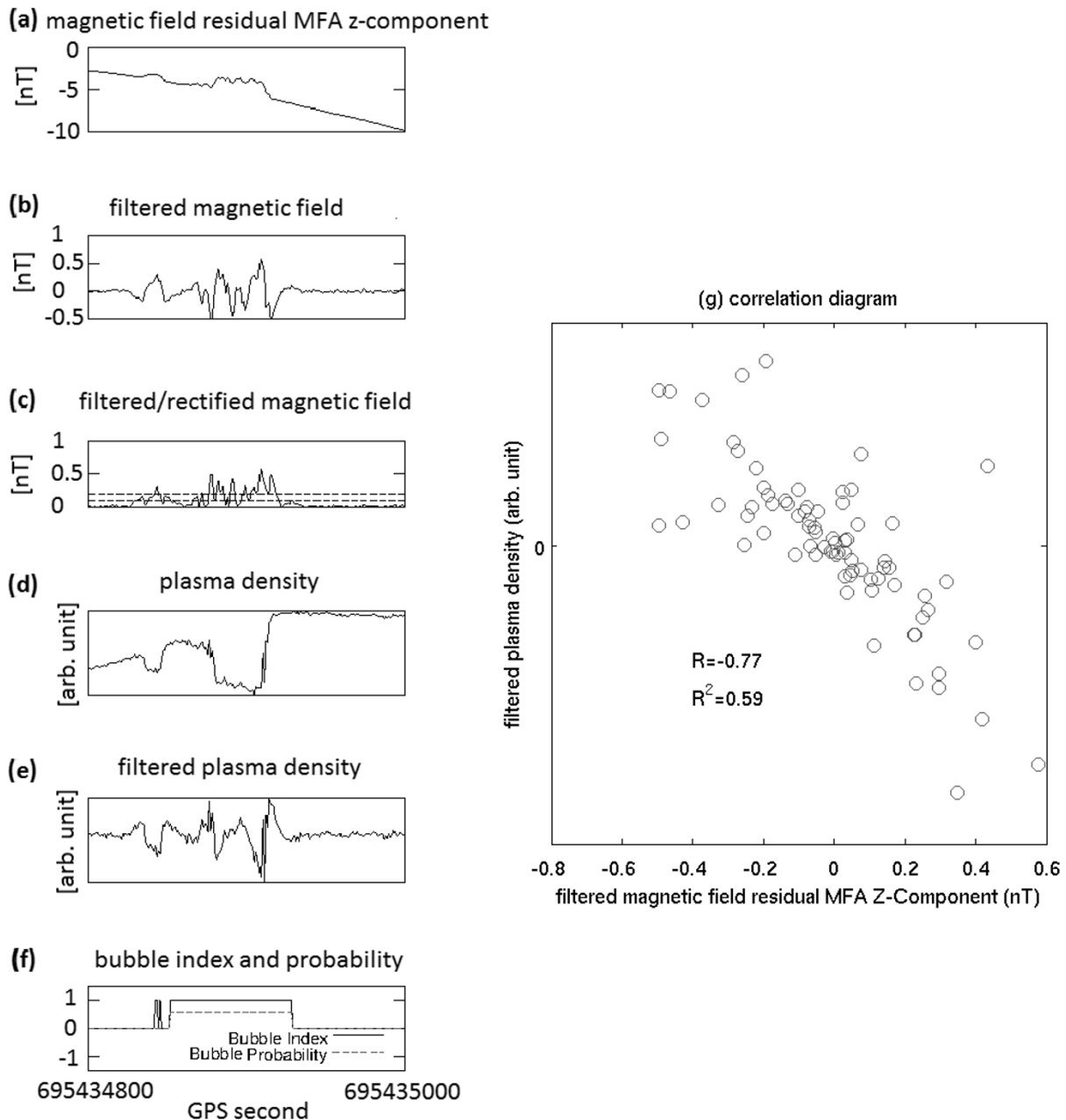


Fig. 1. Illustration of the different processing steps for EPB detection: (a) residual strength, (b) filtered residual strength, (c) filtered/rectified residual strength, (d) plasma density, (e) filtered plasma density, (f) Bubble Index and Bubble Probability, and (g) scatter plot of filtered residual strength and filtered plasma density for the widest EPB in panel (f).

nT): see the upper dashed line in Fig. 1(c). Fluctuations exceeding the threshold are considered as an event. If two events are separated by less than a certain time interval (e.g., 60 seconds), they are merged to one event including the interval in-between. An event can be considered as an ‘EPB’ if it first satisfies the following morphological criteria (Stolle *et al.*, 2006): fluctuations should not stand alone, but be accompanied by similar fluctuations in the surrounding (i.e. data points above the lower dashed line in Fig. 1(c)) as well as by calm background (i.e. data points below the lower dashed line in Fig. 1(c)). Our EPB detection approach goes one step beyond that of Stolle *et al.* (2006) by considering also the concurrent change in plasma density. In this final step filtered residual strength (Fig. 1(b)) and plasma density

filtered in the same way (Fig. 1(e)) are correlated around the detected events (Fig. 1(g)). If the square of the correlation coefficient (the ‘Bubble Probability’: see Subsection 3.3 for details) is higher than a certain threshold (e.g., 0.5), which confirms the diamagnetic effect, the event is deemed a ‘Confirmed Bubble’. In Fig. 1(f) a ‘Confirmed Bubble’ appears with Bubble Index 1 with nonzero Bubble Probability: detailed descriptions of the Bubble Index and the Bubble Probability will be given in Section 3. If (1) the square of the correlation coefficient is lower than the threshold, (2) there is no plasma density data, or (3) the morphological criteria are not satisfied, the event remains an ‘Unconfirmed Bubble’. In Fig. 1(f) an ‘Unconfirmed Bubble’ appears with Bubble Index 1 and Bubble Probability 0. If

Table 1. The list of parameters contained in the L2-IBI data product.

Component	Description
Timestamp	Time stamp in UTC
Latitude	Geographic latitude
Longitude	Geographic longitude
Radius	Geographic radius
Bubble Index	Plasma Bubble Index
Bubble Probability	Probability of the Plasma Bubble Index
Flags Bubble	Flags related to the Plasma Bubble Index
Flags F	Flags characterizing the magnetic field intensity measurement (zero is nominal), passed through from the L1b data
Flags B	Flags characterizing the magnetic field vector measurement (zero is nominal), passed through from the L1b data
Flags q	Flags characterizing the attitude information (zero is nominal), passed through from the L1b data

data points are obtained outside the night-side low-latitude region, or if the data quality of the filtered residual strength is poor (see Subsection 3.2 for details), the corresponding data are considered as ‘Unanalyzable’: Bubble Index -1 .

There are a number of free parameters that can be optimized throughout the *Swarm* lifetime. For example, the event detection threshold (e.g. 0.2 nT) or the time gap needed to separate adjacent EPBs (e.g., >60 seconds) will be optimized according to the actual noise level and quality of the *Swarm* L1b data. The detection threshold of various non-EPB events (‘Unanalyzable’ data: to be described in the following sections) can also be modified.

Note that this automatic detection algorithm cannot distinguish EPBs from plasma blobs which are localized plasma density enhancements (e.g. *Le et al.*, 2003). The events identified by the L2-IBI processor thus contain also blob events. However, the occurrence probability of EPBs is significantly higher than that of blobs during solar maximum years (e.g. *Watanabe and Oya*, 1986, figure 3). During solar minimum years the two occurrence rates can become comparable: the former may even be lower than the latter for some locations and seasons (e.g. *Choi et al.*, 2012, figures 3–4). Therefore, the L2-IBI product during solar minimum may contain significant contribution from plasma blobs as well as from EPBs. With the help of plasma density profiles observed by the *Swarm*/EFI users can distinguish whether a ‘Confirmed Bubble’ in the L2-IBI product originates from EPBs or blobs. An automatic distinction between EPB and blob will be considered in a future development of the algorithm, whose performance can be verified as soon as *Swarm* data will be available.

3. Description of the L2-IBI Product

In this section we describe the format of the L2-IBI data product in detail. The main purpose of the L2-IBI product is, as stated above, to flag whether a magnetic field measurement is affected by EPBs or not. The main part of the L2-IBI product consists of three parameters: Bubble Index, Bubble Flag, and Bubble Probability. The three parameters of the L2-IBI product are assigned to each L1b magnetic field datum (1-second cadence). The remaining parts of the L2-IBI product are auxiliary information such as the observation time, satellite position, and L1b data quality flags.

Table 2. Bubble Index.

Bubble Index	Description
0	Quiet
1	Bubble
-1	Unanalyzable

Table 3. Bubble Flag.

Bubble Flag	Description
0	Quiet
1	Confirmed Bubble
2	Unconfirmed Bubble
4	Jump
8	Data gap
16	Pulsations
32	Outside the night-time low-latitude region

Table 1 gives the parameter list of the L2-IBI data product.

3.1 Bubble Index

The Bubble Index marks every data point as to whether a plasma irregularity is encountered. Table 2 presents the three possible cases of the Bubble Index. Bubble Index 0 (Quiet) signifies that no small-scale fluctuation exists around that data point. Data points of Bubble Index 0 are most appropriate for geomagnetic field modeling. Bubble Index 1 (Bubble) means that the data points are affected by the diamagnetic effect of EPBs. Bubble Index -1 (Unanalyzable) means that either (1) the quality of the L1b data point is poor (e.g. time gap or unphysical jump), or (2) the data is outside the night-time low-latitude range, where we refrain from indexing.

3.2 Bubble Flag

The Bubble Flag (the field name, ‘Flags Bubble’ in Table 1) provides further information as to why the data point is given the Bubble Index. Table 3 lists the meaning of possible Bubble Flags. When the Bubble Index is 0 (Quiet), the corresponding Bubble Flag is also 0 (Quiet). An example for such a case is presented in Fig. 2. The top panel of Fig. 2 shows residual strength obtained from the CHAMP/FGM observations. The second panel presents the filtered residual strength, the rectification (absolute value)

Swarm SW_TEST_IBIATMS_2F 2001 DOY 260 Equatorial Orbit Segment 9

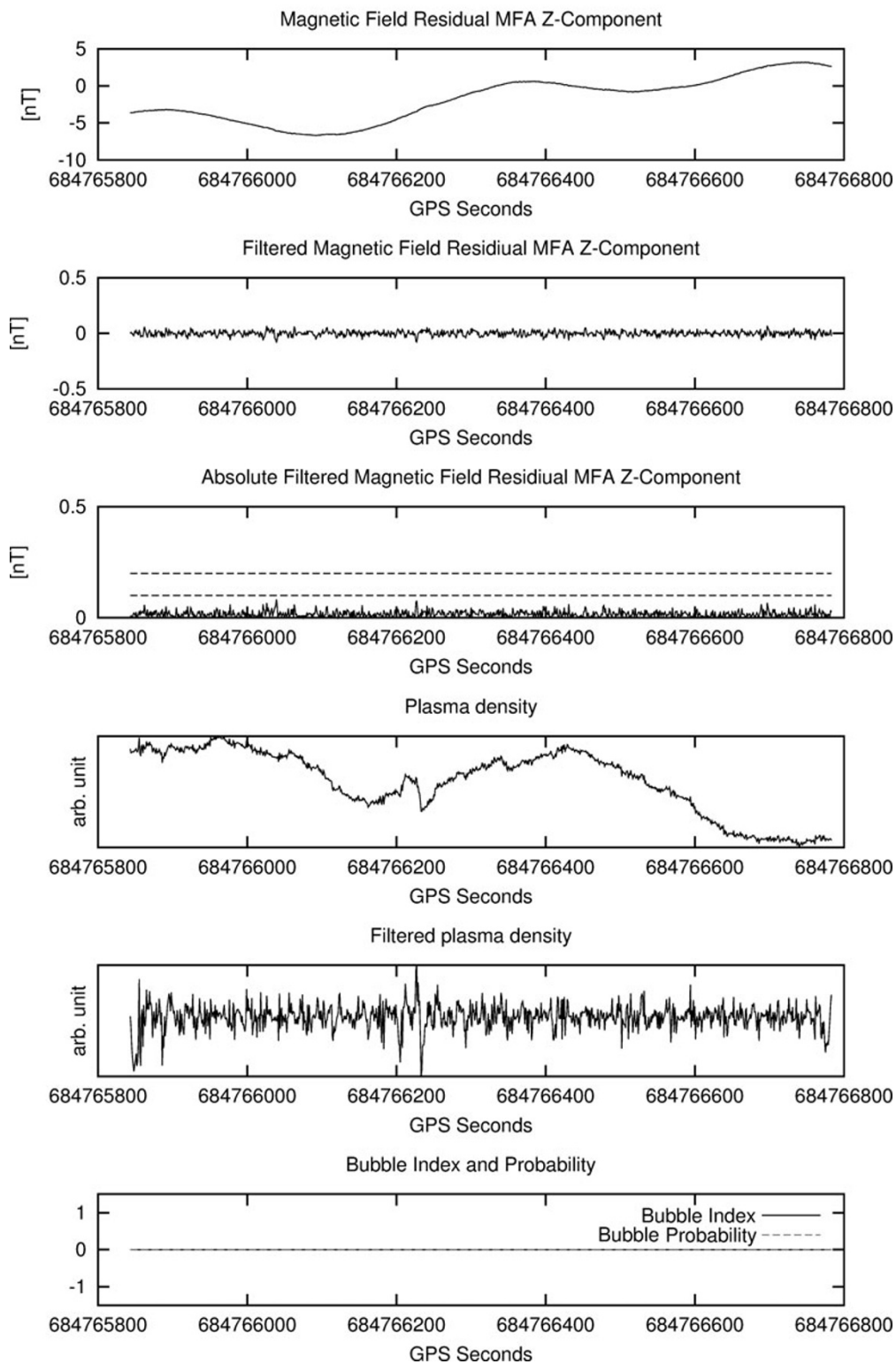


Fig. 2. An example of Bubble Index 0 and Bubble Flag 0 (Quiet). Each panel from top to bottom represents (a) residual strength, (b) filtered residual strength, (c) filtered/rectified residual strength, (d) plasma density, (e) filtered plasma density, and (f) Bubble Index and Bubble Probability, respectively.

of which is shown in the third panel. The fourth panel presents plasma density, as observed by the Digital Ion Drift Meter (DIDM) onboard CHAMP. In the fifth panel is given the DIDM readings filtered by the same high-pass filter as used for the second panel. Note that the DIDM was de-

graded during launch, and the measured plasma density remained uncalibrated. However, the unknown scaling factor and bias hardly affect its correlation with the geomagnetic field residuals. The results obtained by running the L2-IBI processor with the CHAMP data are shown in the bottom

Swarm SW_TEST_IBIATMS_2F 2001 DOY 260 Equatorial Orbit Segment 2

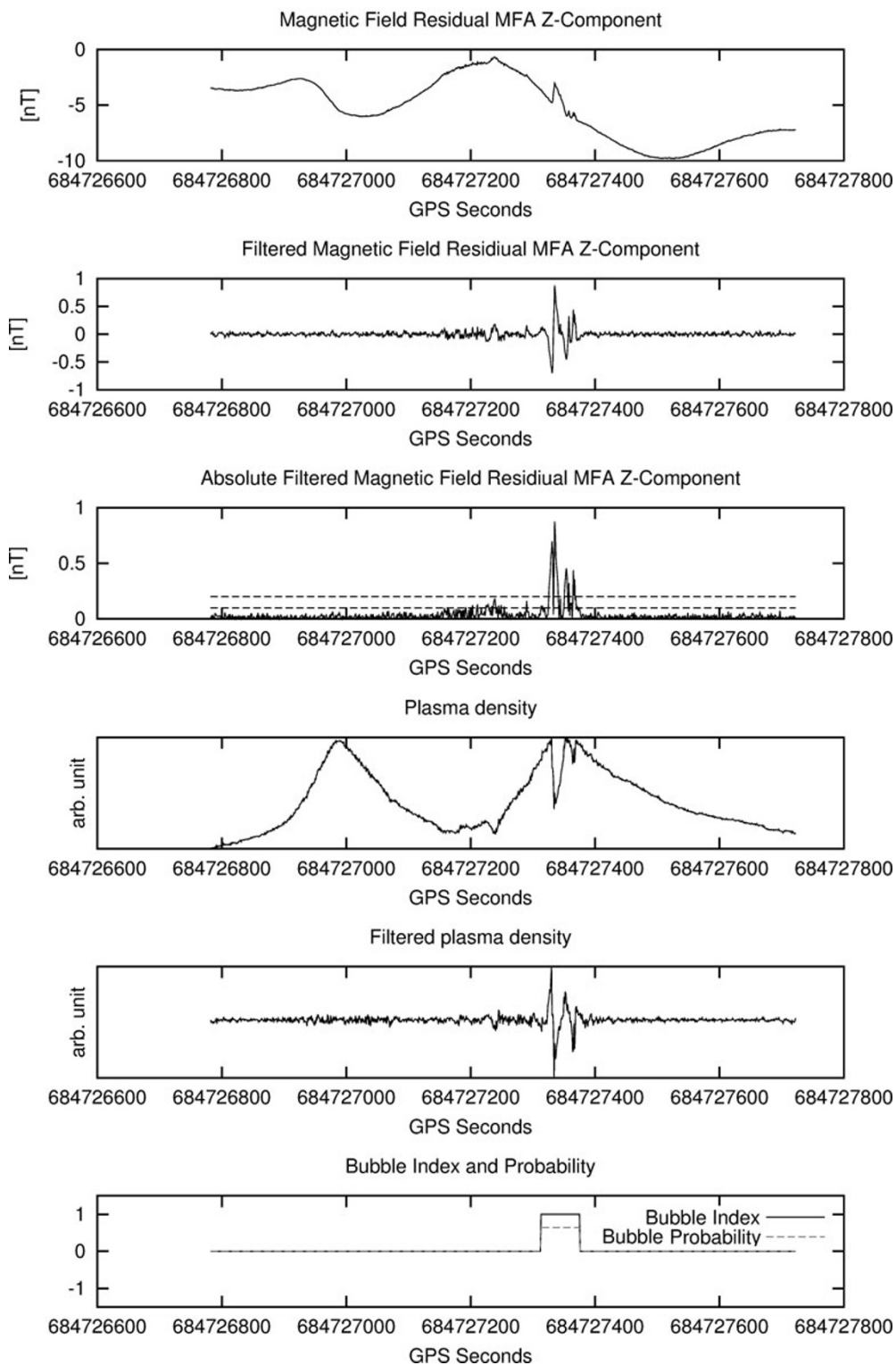


Fig. 3. An example of Bubble Index 1 and Bubble Flag 1 (Bubble). The format is the same as that of Fig. 2.

panel. The solid black line corresponds to the Bubble Index, and the dashed line corresponds to Bubble Probability: the Bubble Probability will be described in detail in Subsection 3.3. We can see that the L2-IBI processor correctly judges that the magnetic data points are unaffected by any significant magnetic fluctuations related to plasma density gradients (Bubble Index 0 and Bubble Probability 0).

If the Bubble Index is 1 (Bubble), then the corresponding Bubble Flag may be either 1 (Confirmed Bubble) or 2 (Unconfirmed Bubble). If an EPB event exhibits high correlation between filtered residual strength and filtered plasma density, Bubble Flag 1 (Confirmed Bubble) is set: see Fig. 3. Otherwise, Bubble Flag is 2 (Unconfirmed Bubble). In Fig. 3 we can see that the L2-IBI processor cor-

Swarm SW_TEST_IBIATMS_2F 2001 DOY 259 Equatorial Orbit Segment 15

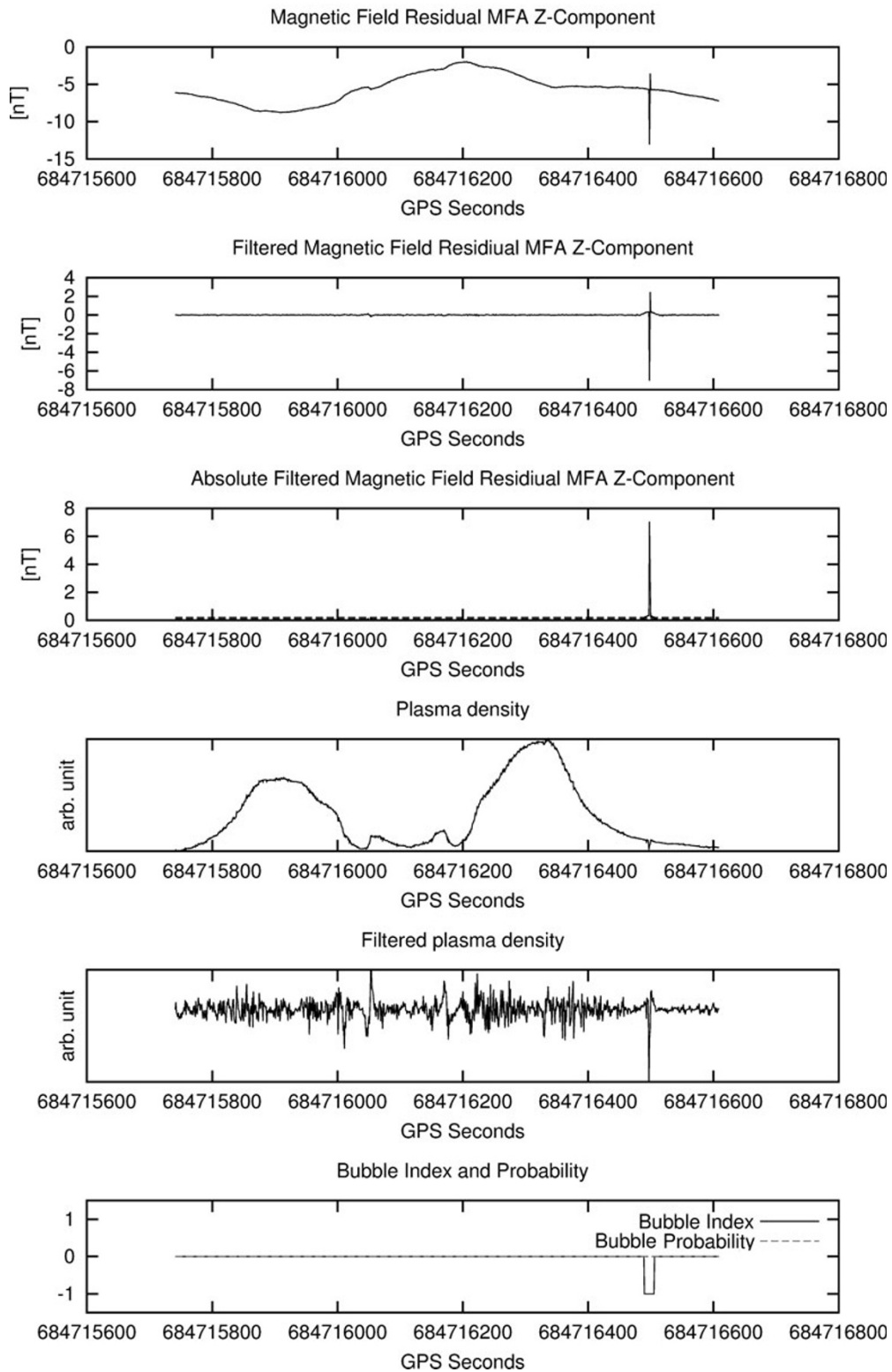


Fig. 4. An example of Bubble Index -1 (Unanalyzable) and Bubble Flag 4 (Jump). The format is the same as that of Fig. 2.

rectly identifies (Bubble Index 1 and Bubble Flag 1) the data points affected by EPBs (i.e. by abrupt plasma density depletions).

If the Bubble Index is -1 (Unanalyzable), the corresponding Bubble Flag value may be between 4 and 32. Outside the night-time low-latitude region the Bubble Flag is

always 32. The Bubble Flag is 4 (Jump) when there is an unphysical jump of the residual strength (e.g., >6 nT: compare this value to typical EPB signatures shown in Stolle *et al.* (2006, figure 2)). In Fig. 4 we can see that the L2-IBI processor correctly identifies the data points affected by the short-duration data jumps, which have little relation to

Swarm SW_TEST_IBIATMS_2F 2001 DOY 324 Equatorial Orbit Segment 5

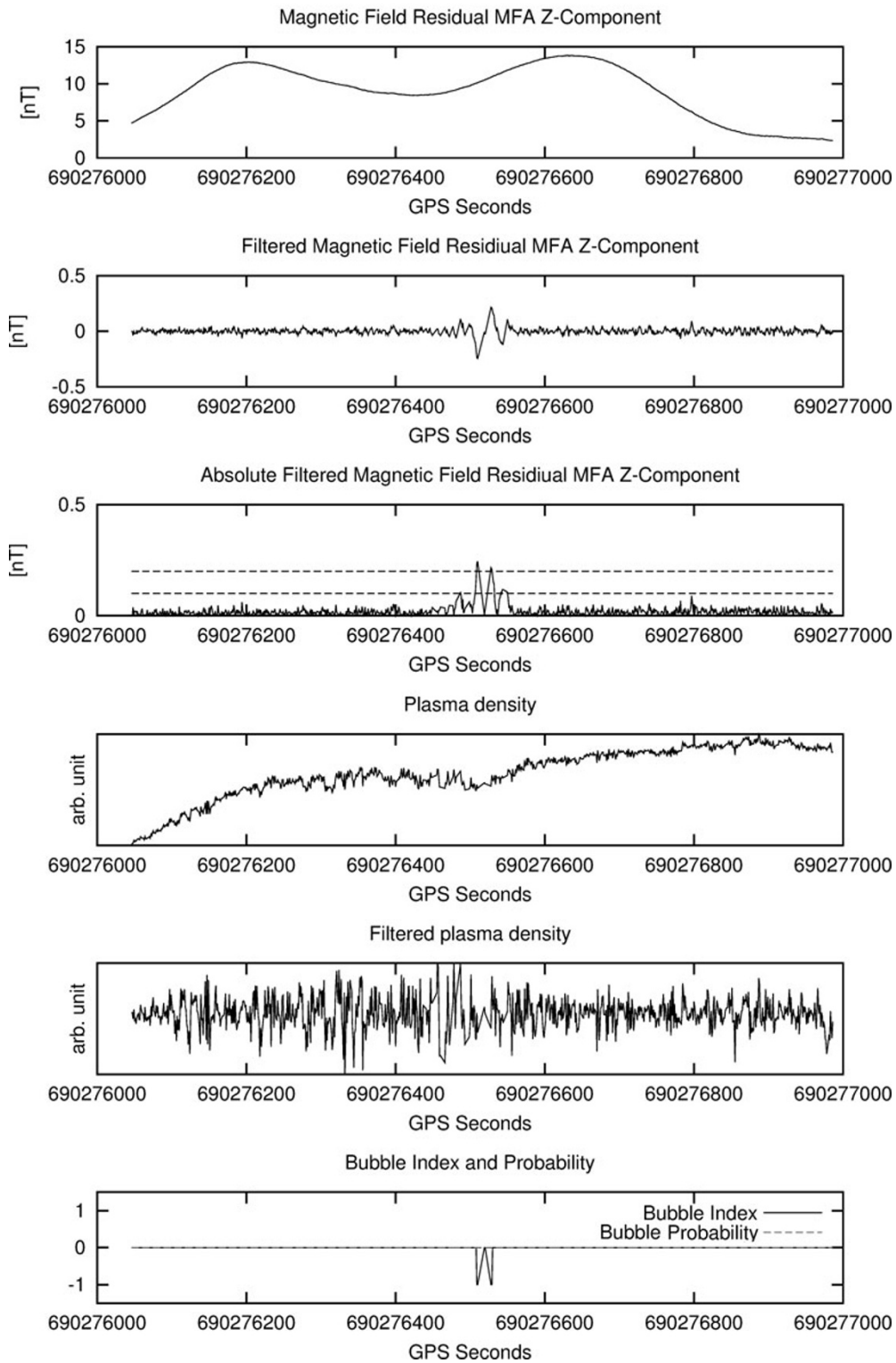


Fig. 5. An example of Bubble Index -1 (Unanalyzable) and Bubble Flag 8 (Time gap). The format is the same as that of Fig. 2.

plasma density variations.

Bubble Flag value is 8 (Data gap) when there are too many (e.g., >12 times) individual gaps or a gap exceeding a certain threshold (e.g., 100 seconds) in the L1b magnetic field data over an orbital arc within $\pm 45^\circ$ GLAT. In Fig. 5 we can see that the L2-IBI processor correctly identifies the data points affected by data gaps, and that the fluctuations

around the time gap actually show no relation to plasma density variations.

When a significant amount (e.g., $>25\%$) of the data points on a night-time low-latitude pass exhibit magnetic fluctuations, it is also deemed unrelated to EPBs. A typical reason for that is magnetic pulsation in the Pc3 range. In that case the Bubble Flag is given the value 16. Figure 6

Swarm SW_TEST_IBIATMS_2F 2002 DOY 013 Equatorial Orbit Segment 9

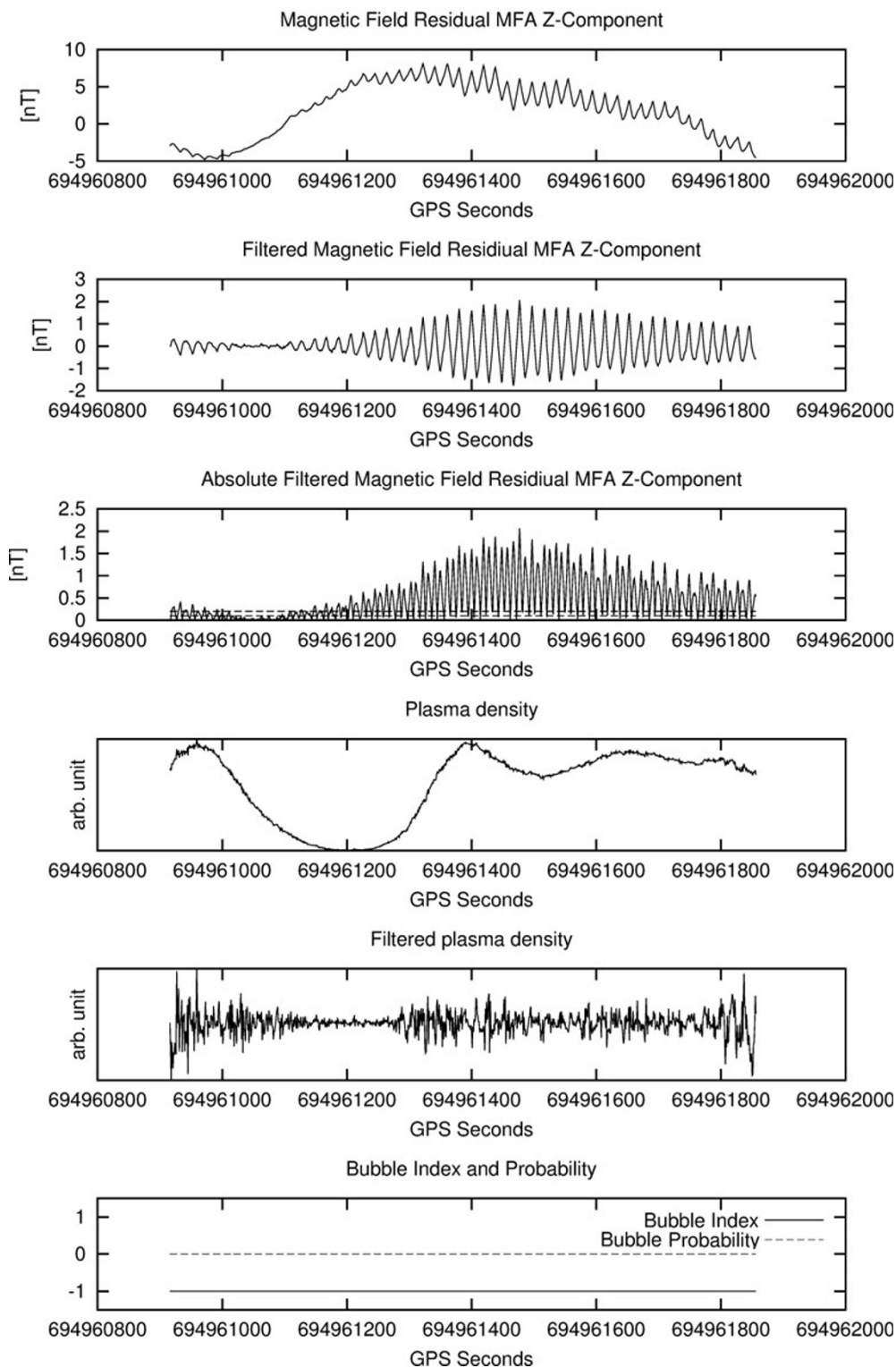


Fig. 6. An example of Bubble Index -1 (Unanalyzable) and Bubble Flag 16 (Pulsations). The format is the same as that of Fig. 2.

shows such an example. Onboard CHAMP the magnetic torque current was modulated by a signal with a period of about 20 seconds. In case of missing torque correction (see Fig. 6) the resulting magnetic variations appear as continuous pulsations, as are correctly indexed in Fig. 6. During those times EPBs cannot be detected properly. For more examples of Unanalyzable data the readers are referred to

Balasis *et al.* (2005).

3.3 Bubble Probability

When the Bubble Index is 1, the L2-IBI processor calculates the correlation coefficient between filtered residual strength and filtered plasma density. The square of the correlation coefficient is used as the Bubble Probability. With higher Bubble Probability it is more probable that the re-

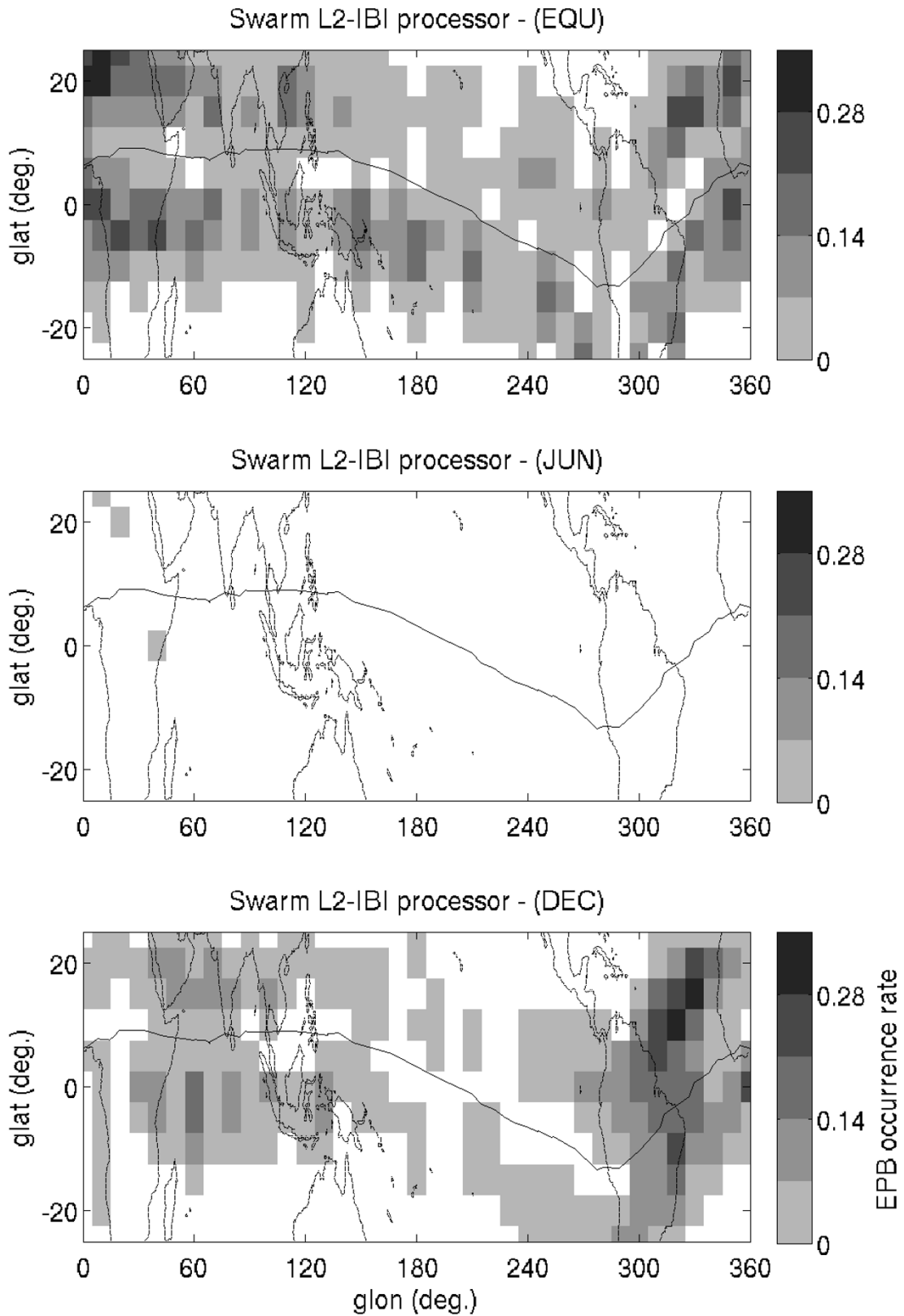


Fig. 7. EPB occurrence rates for equinox, June solstice, and December solstice months, respectively.

lated magnetic field data point is affected by EPBs. As stated above, the Bubble Flag is 1 only if the Bubble Probability exceeds a certain threshold (e.g., 0.5). If the Bubble Index is not 1, or there is no plasma density data around the magnetically detected events ('Unconfirmed Bubble'),

the Bubble Probability is set to 0 automatically. Combining the Bubble Probability and the Bubble Index end users may impose stricter criterion on the correlation between filtered residual strength and filtered plasma density. For example, end users may take only those data points with Bubble In-

dex 1 and Bubble Probability ≥ 0.8 as ‘Confirmed Bubble’.

4. Scientific Validation of the L2-IBI Product

In order to validate the functionality of the L2-IBI processor we have used the CHAMP/FGM and the CHAMP/DIDM data from 126 days in 2001 and 43 days in 2002. The amount of the input data is limited by the difficulty in finding enough DIDM data with reasonable quality.

The L2-IBI data are first binned by GLAT, geographic longitude (GLON), and season. The sizes of the GLAT (GLON) bins are 5° (10°). We divide a year into three seasons: equinox, June solstice, and December solstice. Each solstice season is defined as 131 days around the corresponding solstice day while the combined equinox is defined as the sum of respective 65 days centered around March and September equinoxes. As the $392 (= 131 + 131 + 65 \times 2)$ days exceed the number of days in a year (365 or 366), there are overlaps at the beginning/end of the three seasons. The data of the few overlapping days are counted twice, so that they contribute to the EPB statistics of two seasons. Figure 7 was constructed from 649/355 (pre-midnight/post-midnight) equatorial passes of CHAMP in equinox, 0/448 during June solstice, and 839/551 during December solstice, respectively.

For each GLON-GLAT bin in Fig. 7 the EPB occurrence rate is calculated by dividing the number of EPB data points (Bubble Index 1 and Bubble Flag 1) by that of all the night-time low-latitude CHAMP/FGM data points with good quality (Bubble Index 0 or 1). The result is shown in Fig. 7, which resembles the well-known seasonal-longitudinal (S/L) variation of EPB occurrence (e.g. Stolle *et al.*, 2006; Xiong *et al.*, 2010). During December solstice the occurrence rate is high around Brazil. During June solstice the occurrence rate is lower than during the other seasons; an occurrence peak exists around Africa. During equinox the occurrence rate maximizes near the Atlantic Ocean. All these results are consistent with previous studies on EPBs, and support that the L2-IBI processor correctly identifies EPB events. Note that the general level of occurrence rates in our Fig. 7 is lower than that of Stolle *et al.* (2006, figure 6) although both figures are based on CHAMP data. The difference simply reflects different definitions of occurrence rates, and does not signify inconsistency. In our Fig. 7 the occurrence rates are calculated for each GLAT \times GLON bin while in the case of Stolle *et al.* (2006, figure 6) each CHAMP pass within a GLON bin is considered as a whole.

For June solstice our result is rather poor since we only have data from the post-midnight sector. We note that a secondary peak of occurrence rate, which should appear over the Pacific Ocean (e.g. Stolle *et al.*, 2006, figure 5), is missing. This discrepancy is caused by the limited amount of the CHAMP/DIDM data during June solstice, as mentioned above. The bias of our test data towards the post-midnight sector causes the under-representation in the Pacific region, where EPB activity is known to be stronger during pre-midnight hours than in the post-midnight sector (e.g. Stolle *et al.*, 2008, figure 7). According to our Fig. 7 the maximum EPB occurrence rates are 20–30% except for June solstice. These results are in general agreement with Park

et al. (2009, figure 2). Therefore, the results shown in Fig. 7 exhibit no conflict with previous works. More thorough scientific validation will be conducted during the *Swarm* mission.

5. Conclusion

In this paper we have introduced the *Swarm* L2-IBI product. Using CHAMP observations the L2-IBI production algorithm has been validated scientifically by visual inspection of individual cases (Section 3) and by statistics (Section 4). The L2-IBI product has the following ramifications in the fields of space science and geomagnetism.

- 1) The L2-IBI product can provide the complete EPB list (Bubble Index 1) in the *Swarm* data, so that ionospheric researchers need not strive for implementing complex EPB detection algorithms. Moreover, the information on EPB occurrences is given at two different altitudes of the three *Swarm* satellites, which can expedite EPB studies a lot.
- 2) The L2-IBI product can also give useful constraints to the data selection process in the geomagnetic field modeling. For example, Maus *et al.* (2007) built a geomagnetic field model using the CHAMP/FGM observations, from which the data affected by EPB diamagnetic signatures were excluded. In a similar way, modelers can select *Swarm* L1b data using the *Swarm* L2-IBI product.
- 3) Finally, the algorithm of the L2-IBI production, as described in this paper, can be adapted to ionospheric regimes other than night-time low-latitude ionosphere. For example, ionospheric irregularity at high latitudes or on the dayside may be detected using similar algorithms (e.g. Park *et al.*, 2012).

Acknowledgments. The CHAMP mission was sponsored by the Space Agency of the German Aerospace Center (DLR) through funds of the Federal Ministry of Economics and Technology, following a decision of the German Federal Parliament (grant code 50EE0944). The development of the *Swarm* L2-IBI prototype was sponsored by the ESA (ESTEC) through contract No. 4000102140/10/NL/JA.

References

- Abdu, M. A., R. T. de Medeiros, J. H. A. Sobral, and J. A. Bittencourt, Spread F plasma bubble vertical rise velocities determined from spaced ionosonde observations, *J. Geophys. Res.*, **88**(A11), 9197–9204, doi:10.1029/JA088iA11p09197, 1983.
- Aggson, T. L., H. Laakso, N. C. Maynard, and R. F. Pfaff, In situ observations of bifurcation of equatorial ionospheric plasma depletions, *J. Geophys. Res.*, **101**(A3), 5125–5132, doi:10.1029/95JA03837, 1996.
- Balasis, G., S. Maus, H. Lühr, and M. Rother, Wavelet analysis of CHAMP flux gate magnetometer data, in *Earth Observation with CHAMP: Results from Three Years in Orbit*, edited by C. Reigber *et al.*, pp. 347–352, Springer, New York, 2005.
- Basu, S., K. M. Groves, S. Basu, and P. J. Sultan, Specification and forecasting of scintillations in communication/navigation links: Current status and future plans, *J. Atmos. Sol.-Terr. Phys.*, **64**, 1745–1754, 2002.
- Booker, H. G. and H. W. Wells, Scattering of radio waves in the F-region of ionosphere, *Terr. Mag. Atmos. Elec.*, **43**, 249–256, 1938.
- Burke, W. J., L. C. Gentile, C. Y. Huang, C. E. Valladares, and S. Y. Su, Longitudinal variability of equatorial plasma bubbles observed by DMSP and ROCSAT-1, *J. Geophys. Res.*, **109**, A12301, doi:10.1029/2004JA010583, 2004.
- Choi, H.-S., H. Kil, Y.-S. Kwak, Y.-D. Park, and K.-S. Cho, Comparison of the bubble and blob distributions during the solar minimum, *J. Geophys.*

- Res.*, **117**, A04314, doi:10.1029/2011JA017292, 2012.
- Huang, C. Y., W. J. Burke, J. S. Machuzak, L. C. Gentile, and P. J. Sultan, DMSP observations of equatorial plasma bubbles in the topside ionosphere near solar maximum, *J. Geophys. Res.*, **106**(A5), 8131–8142, doi:10.1029/2000JA000319, 2001.
- Kil, H., S.-Y. Su, L. J. Paxton, B. C. Wolven, Y. Zhang, D. Morrison, and H. C. Yeh, Coincident equatorial bubble detection by TIMED/GUVI and ROCSAT-1, *Geophys. Res. Lett.*, **31**, L03809, doi:10.1029/2003GL018696, 2004.
- Le, G., C.-S. Huang, R. F. Pfaff, S.-Y. Su, H.-C. Yeh, R. A. Heelis, F. J. Rich, and M. Hairston, Plasma density enhancements associated with equatorial spread F: ROCSAT-1 and DMSP observations, *J. Geophys. Res.*, **108**(A8), 1318, doi:10.1029/2002JA009592, 2003.
- Lühr, H., M. Rother, S. Maus, W. Mai, and D. Cooke, The diamagnetic effect of the equatorial Appleton anomaly: Its characteristics and impact on geomagnetic field modeling, *Geophys. Res. Lett.*, **30**(17), 1906, doi:10.1029/2003GL017407, 2003.
- Martinis, C., J. V. Eccles, J. Baumgardner, J. Manzano, and M. Mendillo, Latitude dependence of zonal plasma drifts obtained from dual-site airglow observations, *J. Geophys. Res.*, **108**, 1129, doi:10.1029/2002JA009462, 2003.
- Maus, S., H. Lühr, M. Rother, K. Hemant, G. Balasis, P. Ritter, and C. Stolle, Fifth-generation lithospheric magnetic field model from CHAMP satellite measurements, *Geochem. Geophys. Geosyst.*, **8**, Q05013, doi:10.1029/2006GC001521, 2007.
- Miller, E. S., J. J. Makela, K. M. Groves, M. C. Kelley, and R. T. Tsunoda, Coordinated study of coherent radar backscatter and optical airglow depletions in the central Pacific, *J. Geophys. Res.*, **115**, A06307, doi:10.1029/2009JA014946, 2010.
- Nishioka, M., Su. Basu, S. Basu, C. E. Valladares, R. E. Sheehan, P. A. Roddy, and K. M. Groves, C/NOFS satellite observations of equatorial ionospheric plasma structures supported by multiple ground-based diagnostics in October 2008, *J. Geophys. Res.*, **116**, A10323, doi:10.1029/2011JA016446, 2011.
- Oyama, K.-I., K. Schlegel, and S. Watanabe, Temperature structure of plasma bubbles in the low latitude ionosphere around 600 km altitude, *Planet. Space Sci.*, **36**(6), 553–567, doi:10.1016/0032-0633(88)90025-6, 1988.
- Park, J., C. Stolle, H. Lühr, M. Rother, S.-Y. Su, K. W. Min, and J.-J. Lee, Magnetic signatures and conjugate features of low-latitude plasma blobs as observed by the CHAMP satellite, *J. Geophys. Res.*, **113**, A09313, doi:10.1029/2008JA013211, 2008.
- Park, J., H. Lühr, C. Stolle, M. Rother, K. W. Min, and I. Michaelis, The characteristics of field-aligned currents associated with equatorial plasma bubbles as observed by the CHAMP satellite, *Ann. Geophys.*, **27**, 2685–2697, 2009.
- Park, J., R. Ehrlich, H. Lühr, and P. Ritter, Plasma irregularities in the high-latitude ionospheric F-region and their diamagnetic signatures as observed by CHAMP, *J. Geophys. Res.*, **117**, A10322, doi:10.1029/2012JA018166, 2012.
- Paul, A., B. Roy, S. Ray, A. Das, and A. DasGupta, Characteristics of intense space weather events as observed from a low latitude station during solar minimum, *J. Geophys. Res.*, **116**, A10307, doi:10.1029/2010JA016330, 2011.
- Stolle, C., H. Lühr, M. Rother, and G. Balasis, Magnetic signatures of equatorial spread F as observed by the CHAMP satellite, *J. Geophys. Res.*, **111**, A02304, doi:10.1029/2005JA011184, 2006.
- Stolle, C., H. Lühr, and B. G. Fejer, Relation between the occurrence rate of ESF and the equatorial vertical plasma drift velocity at sunset derived from global observations, *Ann. Geophys.*, **26**, 3979–3988, doi:10.5194/angeo-26-3979-2008, 2008.
- Watanabe, S. and H. Oya, Occurrence characteristics of low latitude ionosphere irregularities observed by impedance probe on board the Hinotori satellite, *J. Geomag. Geoelectr.*, **38**(2), 125–149, 1986.
- Xiong, C., J. Park, H. Lühr, C. Stolle, and S. Y. Ma, Comparing plasma bubble occurrence rates at CHAMP and GRACE altitudes during high and low solar activity, *Ann. Geophys.*, **28**, 1647–1658, doi:10.5194/angeo-28-1647-2010, 2010.
- Xiong, C., H. Lühr, S. Y. Ma, C. Stolle, and B. G. Fejer, Features of highly structured equatorial plasma irregularities deduced from CHAMP observations, *Ann. Geophys.*, **30**, 1259–1269, doi:10.5194/angeo-30-1259-2012, 2012.
- Yokoyama, T., R. F. Pfaff, P. A. Roddy, M. Yamamoto, and Y. Otsuka, On postmidnight low-latitude ionospheric irregularities during solar minimum: 2. C/NOFS observations and comparisons with the Equatorial Atmosphere Radar, *J. Geophys. Res.*, **116**, A11326, doi:10.1029/2011JA016798, 2011.

J. Park (e-mail: park@gfz-potsdam.de), M. Noja, C. Stolle, and H. Lühr